Effect of chromium doping on high temperature tribological properties of silicon-doped diamond-like carbon films

Bruno J. Rodriguez[1,2,*], Tara L. Schiller[1], Daniela Proprentner[1], Marc Walker[3], C.T.John Low[1], Barbara Shollock[1,a], H.Sun[4] and Parnia Navabpour[4,*]

[1] WMG, University of Warwick, Coventry, CV4 7AL, UK

[2] Diamond Science and Technology CDT, University of Warwick, Coventry, CV4 7AL, UK

[3] Department of Physics, University of Warwick, Coventry, CV4 7AL, UK

[4] Teer Coatings Ltd., West Stone House, Berry Hill Industrial Estate, Droitwich, WR9 9AS, UK

ABSTRACT

Amorphous carbon films were deposited by means of closed-field unbalanced magnetron sputtering (CFUBMS). The silicon content was fixed at 1.3 at. %, while the chromium content was increased by modification of the current applied to the chromium magnetrons, with two doping levels, 0.3 and 2.7 at. %. Both, hardness and thermal stability were found to decrease as result of increasing chromium. Ball-on-disk tests revealed friction coefficients of 0.06 at room temperature with similar specific wear rate in all films (~ 4×10^{-13} m^3 N^{-1} m^{-1}). Increasing annealing temperatures were found to reduce the coefficient of friction compared to room temperature values, while increasing the specific wear rate for all films.

KEYWORDS

Diamond-like, high-temperature, Raman, X-ray photoelectron

1. Introduction

Amorphous carbon coatings (a-C) are a metastable form of carbon with a wide range of applications due to their exceptional properties, such as chemical inertness, smoothness, high hardness, low friction and wear resistance [1]. These films have particular advantages in demanding applications, such as high performance tools, atomic microscope probes or hard disks [2,3]. Their outstanding tribological properties allow their application not only in the automotive sector [4–7], where they provide reductions in fuel consumption and CO_2 emissions [2], but also in harsh environmental conditions, such as the ones found in the low earth orbit [8]. Nevertheless, these films have several limitations, such as residual stresses that may lead to adhesion failure [9], thermal stability [10], fracture toughness [11] or the humidity and gaseous environment under which the contact occurs [12,13].

Several dopants, both non-metallic [14–16] and metallic [17–22], have been previously investigated to overcome such drawbacks. Silicon has been reported to have an effect on the residual stresses of the films [23] and reduce the hardness up to a certain silicon content threshold in films without hydrogenated precursors [23,24]. The tribological properties have also been reported to be enhanced by silicon doping, reducing the coefficient of friction with increasing silicon content both at room temperature and high temperatures [25,26] due to the formation of silicon oxides on the sliding surface [27,28].

Among the metallic dopants, chromium is known by its ability to form carbide nanoparticles within the carbon matrix. Chromium (a-C:Cr) doping has also been related to reduction in the residual stresses [29,30] and friction [4,30–32], while increasing the critical load [4,31,32] and fostering cluster formation as the content increases [33]. Different tribological behaviours have been reported under high temperatures for such dopants compared to non-doped films. The wear rate of these films has been reported to increase with increasing chromium content [34], while friction may be reduced with small chromium contents at high temperatures [33]. As for Si-Cr co-doping, Staia *et al.* [35] reported super-low friction values for temperatures as high as 450 ºC although the doping levels were not reported..

In this work, we investigate the properties of chromium, silicon co-doped films deposited using closed-field unbalanced magnetron sputtering (CFUBMS), and the effect of

chromium additions on thermal stability of silicon-doped films as well as their mechanical and tribological properties.

2. Experimental methods

Amorphous carbon films with high sp^2 carbon content were deposited at Teer Coatings Ltd. (Worcestershire, UK) using closed-field unbalanced magnetron sputtering equipment, Teer UDP-1250a. Circular AISI M42 high speed steel specimens of 30 mm diameter were used as substrates for the mechanical testing and steel foils were used for the chemical testing. Prior to deposition, all substrates were thoroughly cleaned in an ultrasonic bath with acetone for 10 minutes and dried using a hot air dryer.

Six identical rectangular magnetron sputtering sources with an area of 1995 cm^2 were used during the deposition with three pyrolytic carbon targets, two chromium targets (purity 99.5%), which were situated in front of each other and one silicon target (purity 99.999%). A carousel was mounted inside the chamber, allowing two-axis rotation. The coating thickness was measured by means of Calotest and displayed an overall thickness of 2.5 ± 0.2 µm. The films consisted of a Cr thin layer that improved the adhesion to the substrate, a gradient CrCSi layer and an outer a-C:Si or a-C:Si,Cr layer. The current applied to the targets varied among the different films, affecting the atomic content of each element, which were measured via x-ray photoelectron spectroscopy (XPS).

Ball-on-disk experiments were carried out using a Multi-Function Tribometer MFT-5000 (Rtec Instruments, Inc., San Jose, CA, USA) and 6.3 mm diameter Al_2O_3 balls as counterpart. The temperature was controlled on the surface of the samples to ensure that the desired temperature was achieved. The tests started 40 min after the temperature was reached to provide sufficient temperature homogenization. The load applied was 10 N, while a frequency of 1 Hz and a linear speed of 1 cm s^{-1} were employed. The tests were carried out at increasing temperatures until the counterpart reached the substrate. Wear was measured by means of an Alicona InfiniteFocus instrument (Alicona Imagine GmbH, Graz, Austria) and specific wear rates were obtained by the relationship between the volume of material lost in the wear track and the product of the applied load and the sliding distance in five different measurements along the wear track.

Hardness and elastic moduli of the different films were determined by means of nano-indentation using NanoTest Xtreme (Micromaterials Ltd., Wrexham, UK) with a diamond

Berkovich indenter. The mean hardness and reduced Young's modulus were obtained from a minimum of 20 indentations. The indentation depth was limited to 200 nm, which is below a tenth of the coating thickness and aided minimising the influence of both surface roughness and substrate on the measured mechanical properties. The Oliver and Pharr [36] method was used to extract the reduced elastic modulus and hardness from the load-displacement curves.

Raman spectroscopy measurements were performed using an inVia reflex Raman microscope (Renishaw PLC., Wotton–under–Edge, UK). The data was recorded using 1800 line/mm rotating grating and Cobolt solid-state laser (λ = 514 nm) through a 20× objective lens. The laser power was limited to 2 mW to avoid damaging the films surface. The spot size was limited to 5 µm and the spectra were recorded for 10 s during 10 accumulations, from 300 cm^{-1} to 2400 cm^{-1}. High temperature measurements were performed in air using a TS 1500 Linkam hot stage (Linkam Scientific Instrument, Tadworth, UK). The spectra were recorded at different specimen temperatures (25, 100, 150, 200, 250, 300, 350 and 400 ºC) with a heating rate of 10 ºC /min. The spectra presented in this work were fitted using a double Gaussian model to ease the comparison with literature.

The chemical composition and bonding states of the carbon were analysed by means of XPS. The first batch were bombarded with Ar^+ ions for a total of 1 hour to remove the surface contaminants. Measurements were taken every 5 minutes and allowed the estimation of the relative sp^3/sp^2 ratio of the bulk film. The second batch were annealed in vacuum for 15 minutes at four different temperatures, 250 ºC, 300 ºC, 350 ºC and 400 ºC. The first set of measurements was carried out in a Kratos Axis Ultra DLD (Kratos Analytical, Manchester, UK). The second set was made using an Omicron Nanotechnology Multiprobe system (Omicron NanoTechnology GmbH, Taunusstein, Germany). The work function and binding energy scale of both spectrometers were calibrated before any experiment against the Fermi edge and $3d_{5/2}$ peak of a polycrystalline Ag sample. In the case of the compositional analysis, clean metallic foils were used to determine the analyser transmission function and the detection efficiency. Al Kα ($h\upsilon$ =1486.7 eV) x-ray beams were used in both cases. The CasaXPS software was used for peak fitting with Voigt mixed Gaussian−Lorentzian line shapes, asymmetry parameters included for the sp^2 carbon component, and the background of each analysed photoelectron emission band was subtracted using the Shirley method [37].

3. Results and discussion

3.1. As-deposited characterisation

The silicon and chromium content of each film was modified through variations in the current applied to the targets. The same bias voltage and silicon target current were used during the deposition of the different films and all inherent changes in content were due to the addition of chromium.

XPS measurements of the as-deposited films were employed to measure the bonding states of C and Si through the estimation of the binding energies (BE) of the C 1*s* and Si 2*p* peaks. Measurements of the bulk film were also obtained through an Ar^+ sputtering process that removed the majority of oxides on the surface. The C 1*s* core-level spectrum was deconvoluted into four main features; carbon sp^2 contribution, carbon sp^3 contribution, silicon/chromium carbides and residual surface contaminants. The sp^2-bonded carbon was centred at 284.3 eV and represented roughly 60-70% of the peak total area. The sp^3 bonded-carbon peak area ratio is shown in Table 1 and was found to vary according to the doping, 18-22 %. This peak was separated by 0.9 eV from the latter, in agreement with prior results presented elsewhere for hydrogen-free carbon films through the comparison with electron energy loss spectroscopy (EELS) [38–40]. Any chromium doping was found to reduce the sp^3 carbon content of the films, as shown in table 1. Silicon and chromium carbides were present at similar energies, 283.5 eV [19], which complicated their differentiation. Nonetheless, the relative area of such peak varied from 4.2 % to 8.2 % in a-C:Si,Cr (1) and a-C:Si,Cr (2) respectively, while the silicon carbide area in a film with similar silicon content, a-C:Si was found to be 2.2 %. Films with high chromium and low silicon content have been reported to display Cr_xSi compounds [19], although these compounds were not found in the present work, probably due to the reduced content of both elements. Surface contaminants were found between 286 eV and 290 eV in the form of oxygen functional groups, such as carboxylic and carbonyl (C-O and C=O) [40,41].

The deconvolution of the bulk coating Si 2*p* peak was studied for all the samples at room temperature before and after the Ar^+ sputtering of the surface. The spectra of the non-sputtered solely silicon-doped films were dominated by Si-O-C, but both SiO_x (103 eV – 105 eV) and Si-C bonds were present. Chromium doping induced a shift in the Si 2*p* peak and was found to reduce the fraction of Si-O-C bonds by 10 %, while the relative area of

Si-C increased with chromium doping (Fig. 1a). The spectra acquired through Ar^+ sputtering of the surface were represented by two main photoelectron emission lines, as shown in Fig. 1b. The main emission line represented 80 % of the spectra and accounted for the silicon bonded with carbon atoms, in the form of Si-C bonds, centred at 100.3 eV. The second emission line, at 101.6 eV, represented the silicon oxide mixed bonds, Si-O-C, which has been attributed effects in the friction properties [42]. The three films presented similar relative areas for each of the emission lines. Non-sputtered films reported in the literature [43,44] have displayed different Si 2*p* peaks and three variable photoelectron emission lines depending upon doping. The non Ar^+ sputtered measurements are in agreement with those presented by other authors using angle-resolved XPS (ARXPS) [25], where improved surface sensitivity was achieved by increasing the take-off angle. Furthermore, reduced take-off angle measurements provided information from greater depth, similarly to the measurements obtained from the bulk of the coating using Ar^+ sputtering

The hardness values are summarized in Table 1. These properties were found to decrease as result of the silicon doping to 16.1 ± 1.0 GPa and 182.7 ± 7.0 GPa respectively, similar to other non-doped carbon films in the literature [45–47]. The addition of chromium reduced the hardness and reduced Young´s modulus compared to those values of the film solely doped with silicon, 13.5 ± 1 GPa and 160.0 ± 6.3 GPa, despite the increase in the sp^3 carbon content presented earlier. Increasing chromium content was found to induce further reductions in these properties, to 10.4 ± 1 GPa and 145.4 ± 6.0 GPa. The progressive reduction in hardness with doping could be induced by a decrease in residual stresses as well as graphitisation [23,33]. Chromium-doped films displayed the lower H/E ratio, which has previously been related with the higher plasticity of tougher films [48], while a-C-Si displayed a higher H/E ratio often related with improved wear resistance due to a higher elastic strain-to-break [49].

Insert Table 1 near here

Raman spectroscopy is used to investigate the bonding structure of carbon-based films and their domain size [50]. Amorphous carbon coatings display two active modes between 1000 cm^{-1} and 1800 cm^{-1} named D and G respectively (Fig. 2) [51]. The D peak, found at 1350 cm^{-1}, has A_{1g} symmetry and involves the breathing mode of the sp^2 sites in rings [52,53]. On the other hand, the G peak centres at 1580 cm^{-1}, has E_{2g} symmetry and involves

the in-plane stretching vibrations of all pairs of sp^2 atoms in either rings or chains [52,53]. The analysis of the Raman spectra of carbon films renders three main parameters, G peak position, full-width half-maximum of the G peak, FWHM(G), and the intensity ratio between both D and G peaks.

As presented in Table 1, silicon doping was found to induce a blue shift in the G-peak position, increased width and reduced peak ratio from that of the rest. The position of this peak has been previously related with the bond stretching of the sp^2 sites and would present a blue with decreasing sp^3 contents in films that were deposited without hydrogenated precursors [52,54]. The reason for such behaviour has been attributed to changes in the sp^2 configuration, moving from rings to olefinic groups [14,55]. Silicon doping induces the opening of sp^2-carbon rings due to its inability to form π-π^* bonds with carbon atoms, which also provides a blue shift [23,56,57]. In addition, it increases the symmetry of the peak, which leads to an increase in the FWHM(G) [58], promotes the formation of Si-C and sp^3 –hybridised C-C, and reduces the sp^2-carbon clusters size from those of the a-C, reducing the peak ratio [14,23]. Meanwhile, the film with the lower content of chromium, a-C:Si,Cr (1), displayed a red shift with regards to a-C:Si, attributed to a reduction in the internal stress of the film, and a reduction in the FWHM(G). This width has previously been used in the literature to estimate both the mechanical properties and sp^3 carbon content of pure carbon films [59,60]. It is indeed correlated with the carbon hybridisation through the symmetry of the G peak, as it increases with both sp^3 content and FWHM(G) [60,61]. This symmetry may also be related to cluster size reductions and the formation of olefinic groups [54], which bonds are shorter than the aromatic bonds and have higher vibration frequencies [54]. The I_D/I_G ratio of the latter film was also found to increase and might be due to the cluster size increase, previously introduced, as it is directly related to the ratio between both peaks [62].

The higher chromium content specimen, a-C:Si,Cr (2) displayed a larger red shift, a large drop in width and an increased peak ratio. This confirmed the tendency observed in the latter film, the role of chromium as a clustering enhancer [29] and its ability to counterbalance the silicon effect.

3.2. High temperature characterisation

Several temperature steps, ranging from 25 ºC until graphitisation of the films, were applied to study the thermal stability via Raman Spectroscopy. As shown in Fig. 3, the films had a

variable initial stage, which length was defined by the doping and a second stage, where the relaxation took over until the eventual graphitisation and desorption of the film.

The initial stage was observed to be longer for solely silicon-doped films, while chromium-doped films were found to present a shorter stage. The reduction on the thermal stability of the latter films could be attributed to the clustering, previously observed at room temperature, and the progressive rearrangement in the sp^2 carbon phase [63]. The position of the G peak was found to be influenced by the dopants and to increase at different temperatures as result of rehybridisation. Silicon doping was found to delay its degradation until 200 °C, while chromium additions counterbalanced the silicon effect and accelerated the relaxation (150 ºC). Simulation studies [55] have reported silicon addition to reduce the clustering with increasing temperature, which agrees with the results presented in this work, while chromium doping displayed an opposite effect to such behaviour. Increasing sp^3 content has been associated with more stable films at higher temperatures than the ones reported in previously published work [64,65]. This supports the explanation of the thermal stability of the silicon-doped films given its effects on the overall sp^3 network. The peak ratio of the films in this work, I_D/I_G, was found to remain rather steady during the same temperature steps as the position of the G peak and increased past them as a result of the increased presence of ordered aromatic rings [54,66]. Similar trends were observed when analysing the FWHM (G), where the disorder was found to decrease as a result of increasing thermal energy, as the film is becoming graphite-like. Both a-C:Si and a-C:Si,Cr (1) presented a sudden change at 400 ºC, which suggested its failure. The drop in the intensity peak rate at 400 ºC could suggest the transition from NC-graphite into graphite, while the film with the higher chromium content, a-C:Si,Cr (2), presented a lower thermal stability with such a change happening at 300 ºC. Similar results were observed by Ferrari *et al.* [54], who attributed it to an ordering trajectory from a-C to nc-graphite and was attributed to a hydrogen effusion from 400 ºC in ta-C:H films [66]. Nevertheless, such results also reported stable G peak position at 1600 cm^{-1} during several annealing steps, while in this work the G peak position reached its maximum value once the intensity peak ratio dropped. This could be related with the larger sp^3 carbon content and thermal stability of tetrahedral amorphous films.

The as-deposited films were also annealed under high vacuum conditions inside a preparation chamber within the XPS system. The compositions of the films were found to change upon increasing annealing temperatures. The C 1*s* core-level peak was studied, but

the evolution of the relative area of the C-C/C-H was not addressed due to the presence of surface contaminants. Nevertheless, such fraction was observed to drop with increasing temperatures in all the films [67], but the chromium-containing films presented a larger effect at lower temperatures than the solely-silicon doped, in agreement with the results previously presented.

The Si 2*p* peak presented similar bonding states to those of the non Ar^+ sputtered at room temperature as presented in Fig. 4. The relative area of Si-C increased as a result of such annealing in vacuum in all the cases, but the formation of SiO_x bonds was also promoted in the Si,Cr-doped films at the expense of the Si-O-C bond fraction. It was observed that the presence of chromium had a direct impact in this fraction, decreasing it from 64 % in a-C:Si to 17 % in a-C:Si,Cr (2). Such reduction could have dramatic effects on the friction properties and could have affected its reduced thermal stability when compared with its peers, as carbon-silica bonds have been reported to be stronger than carbon-silicon bonds [68].

3.3. Tribological properties

The friction coefficient was investigated for the same temperatures applied during the Raman measurements using an Al_2O_3 balls as counterpart. Results are summarised in Fig. 5a. The films were studied beginning at room temperature up to the temperature at which the counterpart reached the substrate. This was found to be affected by the doping.

Surface contaminants may be removed as result of friction, and hence inherent changes may take place within the film, such as the rupture of the bonds and consequent rehybridisation, both due to annealing temperatures and high-pressure contacts, while transfer layers can be created on the counterpart. All these effects will influence the friction coefficient during the running-in period and steady-state period. All doped coatings reported similar steady state friction coefficient values at room temperature, 0.05, as shown in Fig. 6a. Both a-C:Si and a-C:Si,Cr(1) required about 500 strokes to reach steady state, while a-C:Si,Cr (2) reached it after 1500 strokes. As the temperatures increased, friction dropped significantly. At 150 ºC, a-C:Si,Cr(1) presented the lowest coefficient of friction in this work, 0.009 ± 0.002, while the reduction in friction observed in the other films was less significant. The coefficient of friction of a-C:Si and a-C:Si,Cr(2) was found to be 0.019 ± 0.003 and 0.023 ± 0.002 respectively (Fig. 6b). The duration of running-in was reduced in all cases compared to room temperature behaviour and steady-state was achieved before

500 strokes in doped films. These reductions in the coefficient of friction have been previously attributed to a $sp^3 \rightarrow sp^2$ conversion followed by the ordering of the sp^2 phase of the surface bonding [69]. This graphitisation, caused both by the temperature induced by the tribological contact and the annealing temperature, is also thought to lead to the development of a low shear strength tribolayer containing both carbon material and silicon oxides that have the potential to reduce friction. As consequence, a plausible explanation for the drastic increase in friction halfway through the test of a-C:Si,Cr (2) is the rupture and subsequent creation of a transfer layer, observed in friction studies exposed to different environments [70]. The fluctuations in a-C:Si behaviour have been previously related to unstable transfer layers in such doping [71]. At 200 ºC, the friction increased slightly in the case of the doped films, especially in the case of a-C:Si,Cr (2), which became 0.06 ± 0.01. The running-in was decreased to below 400 strokes for all of them, but a-C:Si,Cr (2) required 800 strokes (Fig. 6c). At 250 ºC, both a-C:Si and a-C:Si,Cr (1) reached steady state before 300 strokes (Fig. 6d), although a-C:Si,Cr (1) exhibited a stable behaviour. Nevertheless, chromium-containing films were found to be more susceptible to the annealing temperatures, in agreement with the results previously presented, which could have caused a progressive graphitisation on the upper layer. It is widely reported that carbon films reduce their hardness with temperature [10,72], and this could lead to an increased removal of material that could have acted as abrasive. The entrapment of the excess material in the contact may have caused the features observed in the wear track for a-C:Si,Cr (1) at this temperature, as can be observed in Fig. 7, where a part of the wear track is presented for each sample and temperature. Meanwhile, the specimens that are subjected to a larger graphitisation and softening, such as a-C:Si,Cr (2), are believed to have been exposed to similar processes, although due to the larger extent of the graphitisation it caused the complete removal of the film as result of the friction. At 300 ºC, a-C:Si had a stable friction coefficient of 0.02 after 400 strokes, while a-C:Si,Cr (1) had a variable friction coefficient below 0.1 until 2000 strokes, when it increased and reached the friction coefficient of the substrate, by 3000 strokes (Fig. 6e). At 350 ºC, a-C:Si was found to fail as result of the experiment, exposing the substrate (Fig. 6f). The area mapping investigation of the wear track at all temperatures carried out by means of EDS did not show significant quantities of Al, potentially transferred from the ball counterpart, which may suggest that it did not act as a wear product.

The evolution of the specific wear rate with temperature was summarised in Fig.5b . At room temperature all the films had similar wear rates, with the a-C:Si presenting the lowest, 3.9×10^{-13} m^3 N^{-1} m^{-1}. Chromium additions increased the specific wear rates, but there was no clear relationship with content at room temperature. At 150 ºC, the specific wear rate increased for all films without a clear relationship with the friction values. However, a-C:Si was found to have the lowest specific wear rate, again, with 5.2×10^{-13} m^3 N^{-1} m^{-1}, while a-C:Si,Cr (1) specific wear rate increased to 1.3×10^{-12} m^3 N^{-1} m^{-1}. As the temperature was increased to 200 ºC, a-C:Si,Cr (1) and a-C:Si,Cr (2) consistently reported higher specific wear rates, with 1.4×10^{-12} m^3 N^{-1} m^{-1} and 4.2×10^{-12} m^3 N^{-1} m^{-1} respectively. At 250 ºC, a-C:Si reported values of 8.7×10^{-12} m^3 N^{-1} m^{-1}, while the substrate was reached in the case of a-C:Si,Cr (2) with an specific wear rate of 1.9×10^{-11} m^3 N^{-1} m^{-1}. At 300 ºC, a-C:Si,Cr (1) failed and the substrate was also reached as a result of the friction. The specific wear rates were found to be 1.4×10^{-11} m^3 N^{-1} m^{-1}, over an order of magnitude larger than the 1.5×10^{-12} m^3 N^{-1} m^{-1} of a-C:Si at the same temperature. These results are in agreement with prior publications that found larger wear rates in solely Cr-doped diamond-like carbon films than in either Si-doped or non-doped with temperature [73] and some other publications that reported increased wear rates with increasing chromium-content [74].

High temperature tribological properties followed the trend defined by Raman spectroscopy in terms of thermal stability with a single step difference between the failures, 50 ºC, which could be due to the time-dependency of these films [75] or even the difference in the experimental set-up between ball-on-disk and high temperature Raman spectroscopy. Silicon, chromium co-doped films were found to consistently report similar friction values to a-C:Si or even lower in the case a-C:Si,Cr (1), which is in agreement with values previously reported for silicon-doped films against Al_2O_3 under different contact pressures [25,73,76,77]. The formation of Si-O compounds, observed in XPS, has previously been attributed lubrication effects [27,28]. Hence they could be responsible for reducing the wear when comparing the films containing chromium in this work with friction values of a-C:Cr coatings reported elsewhere [33,73], both at room and at high temperatures. These chromium additions were also found to induce changes in the Si 2p peak through reductions in the relative area of the silicon oxide bonding emission lines. Such change, could have influenced both the thermal stability of the films and the friction properties [68].

As for the H/E relationship, no effect was observed in the friction properties among the doped films, although the higher H/E specimen, a-C:Si, showed a clear improvement in the wear behaviour compared with the chromium-containing films. Staia *et al.* [35] studied Si,Cr co-doping with contents between 0.5 – 10% at. Cr and 1 – 5 at. % Si and reported low friction values at temperatures as high as 450 ºC. High temperatures would be expected to induce an extended graphitisation and softening, as observed in this work, but the ten-fold reduction in load employed, could have hindered the complete removal of the film. Further comparison was complicated since the actual contents were not disclosed, but according to the Raman spectroscopy results presented in this work, any chromium addition would have a negative effect on the thermal stability and wear rate. This assumption is partially in agreement with a recent publication by Santiago *et al.* [72], where higher chromium contents, than studied here, were considered. It was suggested that the formation of chromium carbide bonds, found to increase by any chromium content, is responsible for the reduction in both mechanical and wear properties, and that it is only when metallic chromium is distributed along the matrix, that the properties are enhanced. The fact that such improvement occurred for chromium contents above values presented in this work, may suggest that Si,Cr co-doped films could benefit from alternative deposition techniques such as HiPIMS.

The failure of the higher chromium containing film, a-C:Si,Cr (2), at 250 ºC occurred in a different manner to the rest of the films since the counterpart reached the substrate, but the coating remained unaffected. This behaviour could be attributed to the reduction in hardness with temperature as previously mentioned. This agrees with the FWHM (G) evolution obtained from Raman spectroscopy and would allow an easier removal of the film by the counterpart. The failure in the rest of the specimens happened through the removal of the film as result of the increased temperature, along with a four-fold increase in roughness that could indicate structural changes.

4. Conclusions

Diamond-like carbon films either non-doped or doped with silicon and chromium were deposited via closed-field unbalanced magnetron sputtering techniques. Both dopants were found to have an effect in the mechanical properties. The hardness was reduced from 16.1 ± 1.0 GPa in the a-C:Si to 10.4 ± 1 GPa in a-C:Si,Cr (2) and the H/E' ratio was reduced with increasing chromium content. Small silicon additions (<1.3 at. %) reduced the cluster

size and had a positive effect in the thermal stability of the films, increasing it, at least by 50 °C, while chromium additions enhanced the clustering behaviour, counterbalanced any silicon effect and reduced the thermal stability. Ball-on-disk tests at 10 N with a Al_2O_3 ball as a counterpart reported friction coefficient values of 0.05 in the doped films. As the temperature was increased, a-C:Si and a-C:Si,Cr (1) consistently displayed low friction coefficient values (< 0.03) from 150 to 300 ºC, reporting the latter super-low friction at 150 ºC (0.009 ± 0.002). As the temperature was increased, silicon, chromium co-doped films consistently reported a larger specific wear rate with increasing chromium doping having a direct effect. It is thought that both effects were induced by the alternative bonding conditions achieved by the presence of chromium.

Acknowledgments

The present work has been supported by the Engineering and Physical Science Research Council (EPRSC) through the Center for Doctoral Training in Diamond Science and Technology (EP/L015315/1). The authors are grateful to Drs. Sue Field, Ben Breeze and Raul Chinchilla for the fruitful discussions.

AUTHOR INFORMATION

Corresponding Authors

*E-mail: B.Rodriguez@warwick.ac.uk, Parnia.Navabpour@teercoatings.co.uk

ORCID

Bruno J. Rodriguez: 0000-0002-5545-3192

PRESENT ADDRESES

[a] B.S..: Department of Engineering, King's College London, London, U.K., WC2R 2LS

References

[1] Donnet C, Erdemir A. Tribology of Diamond-Like Carbon Films: Fundamentals and Applications. 2008. doi:10.1007/978-0-387-49891-1.

[2] Erdemir A, Donnet C. Tribology of diamond-like carbon films: Recent progress and future prospects. J Phys D Appl Phys 2006;39. doi:10.1088/0022-3727/39/18/R01.

[3] Ferrari AC. Diamond-like carbon for magnetic storage disks. Surf Coatings Technol 2004;180–181:190–206. doi:10.1016/j.surfcoat.2003.10.146.

[4] Stallard J, Mercs D, Jarratt M, Teer DG, Shipway PH. A study of the tribological behaviour of three carbon-based coatings, tested in air, water and oil environments at high loads. Surf Coatings Technol 2004;177–178:545–51. doi:10.1016/S0257-8972(03)00925-3.

[5] Jarratt M, Stallard J, Renevier NM, Teer DG. An improved diamond-like carbon coating with exceptional wear properties. Diam Relat Mater 2003;12:1003–7. doi:10.1016/S0925-9635(02)00296-0.

[6] Field SK, Jarratt M, Teer DG. Tribological properties of graphite-like and diamond-like carbon coatings. Tribol Int 2004;37:949–56. doi:10.1016/j.triboint.2004.07.012.

[7] Holmberg K, Erdemir A. Influence of tribology on global energy consumption, costs and emissions. Friction 2017;5:263–84. doi:10.1007/s40544-017-0183-5.

[8] Mangolini F, Krick BA, Jacobs TDB, Khanal SR, Streller F, McClimon JB, et al. Effect of silicon and oxygen dopants on the stability of hydrogenated amorphous carbon under harsh environmental conditions. Carbon N Y 2018;130:127–36. doi:10.1016/j.carbon.2017.12.096.

[9] Santiago JA, Fernández-Martínez I, Wennberg A, Molina-Aldareguia JM, Castillo-Rodríguez M, Rojas TC, et al. Adhesion enhancement of DLC hard coatings by HiPIMS metal ion etching pretreatment. Surf Coatings Technol 2018;349:787–96. doi:10.1016/j.surfcoat.2018.04.090.

[10] Rouhani M, Chau-Nan Hong F, Jeng YR. In-situ thermal stability analysis of amorphous carbon films with different sp3 content. Carbon N Y 2018;130:401–9. doi:10.1016/j.carbon.2018.01.034.

[11] Jungk JM, Boyce BL, Buchheit TE, Friedmann TA, Yang D, Gerberich WW. Indentation fracture toughness and acoustic energy release in tetrahedral amorphous carbon diamond-like thin films. Acta Mater 2006;54:4043–52. doi:10.1016/j.actamat.2006.05.003.

[12] Gilmore R, Hauert R. Control of the tribological moisture sensitivity of diamond-like carbon films by alloying with F, Ti or Si. Thin Solid Films 2001;398:199–204. doi:10.1016/S0040-6090(01)01437-7.

[13] Sánchez-López JC, Erdemir A, Donnet C, Rojas TC. Friction-induced structural transformations of a diamondlike carbon coatings under various atmospheres. Surf Coatings Technol 2003;163–164:444–50. doi:10.1016/S0257-8972(02)00641-2.

[14] Zhao JF, Lemoine P, Liu ZH, Quinn JP, McLaughlin JA. Effects of Si incorporation on the microstructure and nanomechanical properties of DLC thin films. J Phys Condens Matter 2000;12:9201–13. doi:10.1088/0953-8984/12/44/302.

[15] Ogwu AA, Magill D, Maguire P, McLaughlin J, McCullough RW, Voulot D. Nitrogen doping of amorphous DLC films by rf plasma dissociated nitrogen atom surface bombardment in a vacuum. Surf Eng 2000;16:427–30. doi:10.1179/026708400101517422.

[16] Zeng C, Chen Q, Xu M, Deng S, Luo Y, Wu T. Enhancement of mechanical, tribological and morphological properties of nitrogenated diamond-like carbon films by gradient nitrogen doping. Diam Relat Mater 2017;76:132–40. doi:10.1016/j.diamond.2017.05.004.

[17] Gassner G, Mayrhofer PH, Patscheider J, Mitterer C. Thermal stability of nanocomposite CrC/a-C:H thin films. Thin Solid Films 2007;515:5411–7. doi:10.1016/j.tsf.2006.12.149.

[18] Adelhelm C, Balden M, Rinke M, Stueber M. Influence of doping (Ti, V, Zr, W) and annealing on the sp2 carbon structure of amorphous carbon films. J Appl Phys 2009;105. doi:10.1063/1.3075843.

[19] Bertóti I, Tóth A, Mohai M, Szépvölgyi J. Chemical structure and mechanical properties of Si-containing a-C:H and a-C thin films and their Cr- and W-containing derivatives. Surf Coatings

Technol 2011;206:630–9. doi:10.1016/j.surfcoat.2011.05.041.

[20] Sánchez-López JC, Dominguez-Meister S, Rojas TC, Colasuonno M, Bazzan M, Patelli A. Tribological properties of TiC/a-C:H nanocomposite coatings prepared via HiPIMS. Appl Surf Sci 2018;440:458–66. doi:10.1016/j.apsusc.2018.01.135.

[21] Liang CH, Wang WL, Huang CF, Tsai HY, Yang CC. The influence of microstructural variations on mechanical and tribological properties of low-friction TiC/diamond-like carbon nanocomposite films. Ceram Int 2014;40:13329–37. doi:10.1016/j.ceramint.2014.05.047.

[22] Liang CH, Huang CF, Tsai HY. The influence of substrate bias voltages on structure, mechanical properties and anti-corrosion performance of Cr doped diamond-like carbon films deposited by steered cathodic arc evaporation. Thin Solid Films 2015;597:88–96. doi:10.1016/j.tsf.2015.11.010.

[23] Ong SE, Zhang S, Du H, Sun D. Relationship between bonding structure and mechanical properties of amorphous carbon containing silicon. Diam Relat Mater 2007;16:1628–35. doi:10.1016/j.diamond.2007.02.009.

[24] Kulikovsky V, Vorlíček V, Boháč P, Kurdyumov A, Jastrabík L. Mechanical properties of hydrogen-free a-C:Si films. Diam Relat Mater 2004;13:1350–5. doi:10.1016/j.diamond.2003.10.040.

[25] Evaristo M, Azevedo R, Palacio C, Cavaleiro A. Influence of the silicon and oxygen content on the properties of non-hydrogenated amorphous carbon coatings. Diam Relat Mater 2016;70:201–10. doi:10.1016/j.diamond.2016.10.024.

[26] Hatada R, Flege S, Baba K, Ensinger W, Kleebe HJ, Sethmann I, et al. Temperature dependent properties of silicon containing diamondlike carbon films prepared by plasma source ion implantation. J Appl Phys 2010;107. doi:10.1063/1.3394002.

[27] Oguri K, Arai T. Tribological properties and characterization of diamond-like carbon coatings with silicon prepared by plasma-assisted chemical vapour deposition. Surf Coatings Technol 1991;47:710–21. doi:https://doi.org/10.1016/0257-8972(91)90344-V.

[28] Oguri K, Arai T. Two different low friction mechanisms of diamond-like carbon with silicon coatings formed by plasma-assisted chemical vapor deposition. J Mater Res 1992;7:1313–6. doi:https://doi.org/10.1557/JMR.1992.1313.

[29] Savchenko D, Vorlíček V, Prokhorov A, Kalabukhova E, Lančok J, Jelínek M. Raman and EPR spectroscopic studies of chromium-doped diamond-like carbon films. Diam Relat Mater 2018;83:30–7. doi:10.1016/j.diamond.2018.01.021.

[30] Fang L, Shen M. DLC based coatings prepared by reactive d.c. magnetron sputtering. Thin Solid Films 2004:142–7. doi:10.1016/S0040-6090.

[31] Yang S, Teer DG. Investigation of sputtered carbon and carbon/chromium multi-layered coatings. Surf. Coatings Technol., vol. 131, 2000, p. 412–6. doi:10.1016/S0257-8972(00)00859-8.

[32] Yang S, Li X, Renevier NM, Teer DG. Tribological properties and wear mechanism of sputtered C/Cr coating. Surf Coatings Technol 2001;142–144:85–93. doi:10.1016/S0257-8972(01)01147-1.

[33] Zou CW, Wang HJ, Feng L, Xue SW. Effects of Cr concentrations on the microstructure, hardness, and temperature-dependent tribological properties of Cr-DLC coatings. Appl Surf Sci 2013;286:137–41. doi:10.1016/j.apsusc.2013.09.036.

[34] Singh V, Jiang JC, Meletis EI. Cr-diamondlike carbon nanocomposite films: Synthesis, characterization and properties. Thin Solid Films 2005;489:150–8.

doi:10.1016/j.tsf.2005.04.104.

[35] Staia MH, Dubar L, Dubar M, Puchi-Cabrera ES, Iost A, de Baets P, et al. Mechanical characterization of a prototype a-C:Cr,Si and its tribological behavior at high temperature. Tribol Int 2016;100:242–54. doi:10.1016/j.triboint.2016.01.048.

[36] Oliver, W. C. and Pharr GM. An improved technique for determining hardness and elastic modulus using load and displacement sensing indentation experiments. J Mater Res 1992;7:1564–83. doi:10.1557/JMR.1992.1564.

[37] Shirley DA. High-resolution x-ray photoemission spectrum of the valence bands of gold. Phys Rev B 1972;5:4709–14. doi:10.1103/PhysRevB.5.4709.

[38] Díaz J, Paolicelli G, Ferrer S, Comin F. Separation of the sp3 and sp2 components in the C1s photoemission spectra of amorphous carbon films. Phys Rev B 1996;54:8064–9. doi:10.1103/PhysRevB.54.8064.

[39] Möller W. Modeling of the sp3/sp2 ratio in ion beam and plasma-deposited carbon films. Appl Phys Lett 1991;59:2391–3. doi:10.1063/1.106026.

[40] Mérel P, Tabbal M, Chaker M, Moisa S, Margot J. Direct evaluation of the sp 3 content in diamond-like-carbon films by XPS. Appl Surf Sci 1998;136:105–10. doi:10.1016/S0169-4332(98)00319-5.

[41] Zhao JF, Lemoine P, Liu ZH, Quinn JP, Maguire P, McLaughlin JA. A study of microstructure and nanomechanical properties of silicon incorporated DLC films deposited on silicon substrates. Diam Relat Mater 2001;10:1070–5. doi:10.1016/S0925-9635(00)00544-6.

[42] Bhowmick S, Banerji A, Lukitsch MJ, Alpas AT. The high temperature tribological behavior of Si, O containing hydrogenated diamond-like carbon (a-C:H/a-Si:O) coating against an aluminum alloy. Wear 2015;330–331:261–71. doi:10.1016/j.wear.2015.01.072.

[43] Wu WJ, Hon MH. Thermal stability of diamond-like carbon films with added silicon. Surf Coatings Technol 1999;111:134–40. doi:10.1016/S0257-8972(98)00719-1.

[44] Ahmed MH, Byrne JA, Ahmed W. Characteristic of silicon doped diamond like carbon thin films on surface properties and human serum albumin adsorption. Diam Relat Mater 2015;55:108–16. doi:10.1016/j.diamond.2015.03.016.

[45] Lanigan J, Freeman HM, Wang C, Ward MB, Morina A, Neville A, et al. Understanding the wear behaviour of non-doped and Si,O-doped diamond-like carbon films. RSC Adv 2017;7:43600–10. doi:10.1039/C7RA08959G.

[46] Lugo DC, Silva PC, Ramirez MA, Pillaca EJDM, Rodrigues CL, Fukumasu NK, et al. Characterization and tribologic study in high vacuum of hydrogenated DLC films deposited using pulsed DC PECVD system for space applications. Surf Coatings Technol 2017. doi:10.1016/j.surfcoat.2017.07.084.

[47] Pal SK, Jiang J, Meletis EI. Effects of N-doping on the microstructure, mechanical and tribological behavior of Cr-DLC films. Surf Coatings Technol 2007;201:7917–23. doi:10.1016/j.surfcoat.2007.03.036.

[48] Beake BD, Liskiewicz TW, Bird A, Shi X. Micro-scale impact testing - A new approach to studying fatigue resistance in hard carbon coatings. Tribiology Int 2019:1–10. doi:10.1016/j.triboint.2019.04.016.

[49] Leyland A, Matthews A. On the significance of the H / E ratio in wear control : a nanocomposite coating approach to optimised tribological behaviour. Wear 2000;246:1–11. doi:10.1016/S0043-1648(00)00488-9.

[50] Ferrari AC, Robertson J. Resonant Raman spectroscopy of disordered, amorphous, and

diamondlike carbon. Phys Rev B 2001;64:075414. doi:10.1103/PhysRevB.64.075414.

[51] Irmer G, Dorner-Reisel A. Micro-Raman studies on DLC coatings. Adv Eng Mater 2005;7:694–705. doi:10.1002/adem.200500006.

[52] Robertson J. Diamond-like amorphous carbon. Mater Sci Eng 2002;37:129–281. doi:10.1016/S0927-796X(02)00005-0.

[53] Casiraghi C, Piazza F, Ferrari AC, Grambole D, Robertson J. Bonding in hydrogenated diamond-like carbon by Raman spectroscopy. Diam. Relat. Mater., vol. 14, 2005, p. 1098–102. doi:10.1016/j.diamond.2004.10.030.

[54] Ferrari AC, Robertson J. Interpretation of Raman spectra of disordered and amorphous carbon. Phys Rev B 2000;61:14095–107. doi:10.1103/PhysRevB.61.14095.

[55] Hilbert J, Mangolini F, McClimon JB, Lukes JR, Carpick RW. Si doping enhances the thermal stability of diamond-like carbon through reductions in carbon-carbon bond length disorder. Carbon N Y 2018;131:72–8. doi:10.1016/j.carbon.2018.01.081.

[56] He XM, Walter KC, Nastasi M, Lee ST, Fung MK. Investigation of Si-doped diamond-like carbon films synthesized by plasma immersion ion processing. J Vac Sci Technol A Vacuum, Surfaces, Film 2000;18:2143. doi:10.1116/1.1286141.

[57] Racine B, Ferrari AC, Morrison NA, Hutchings I, Milne WI, Robertson J. Properties of amorphous carbon-silicon alloys deposited by a high plasma density source. J Appl Phys 2001;90:5002–12. doi:10.1063/1.1406966.

[58] Zhao F, Li HX, Ji L, Mo YF, Quan WL, Zhou HD, et al. Structural, mechanical and tribological characterizations of a-C : H : Si films prepared by a hybrid PECVD and sputtering technique. J Phys D Appl Phys 2009;42:165407. doi:10.1088/0022-3727/42/16/165407.

[59] Casiraghi C, Ferrari AC, Robertson J. Raman spectroscopy of hydrogenated amorphous carbons. Phys Rev B - Condens Matter Mater Phys 2005;72:1–14. doi:10.1103/PhysRevB.72.085401.

[60] Robertson J. Diamond-like amorphous carbon. Mater Sci Eng R Reports 2002;37:129–281. doi:10.1016/S0927-796X(02)00005-0.

[61] Tamor MA, Vassell WC. Raman “fingerprinting” of amorphous carbon films. J Appl Phys 1994;76:3823–30. doi:10.1063/1.357385.

[62] Tuinstra F, Koenig JL. Raman Spectrum of Graphite. J Chem Phys 1970;53:1126–30. doi:10.1063/1.1674108.

[63] Ferrari AC, Rodil SE, Robertson J, Milne WI. Is stress necessary to stabilise sp3 bonding in diamond-like carbon? Diam Relat Mater 2002;11:994–9. doi:10.1016/S0925-9635(01)00705-1.

[64] Grierson DS, Sumant A V., Konicek AR, Friedmann TA, Sullivan JP, Carpick RW. Thermal stability and rehybridization of carbon bonding in tetrahedral amorphous carbon. J Appl Phys 2010;107. doi:10.1063/1.3284087.

[65] Ferrari AC, Kleinsorge B, Morrison NA, Hart A, Stolojan V, Robertson J. Stress reduction and bond stability during thermal annealing of tetrahedral amorphous carbon. J Appl Phys 1999;85:7191–7. doi:10.1063/1.370531.

[66] Conway NMJ, Ferrari AC, Flewitt AJ, Robertson J, Milne WI, Tagliaferro A, et al. Defect and disorder reduction by annealing in hydrogenated tetrahedral amorphous carbon. Diam Relat Mater 2000;9:765–70. doi:10.1016/S0925-9635(99)00271-X.

[67] Peng J, Sergiienko A, Mangolini F, Stallworth PE, Greenbaum S, Carpick RW. Solid state

magnetic resonance investigation of the thermally-induced structural evolution of silicon oxide-doped hydrogenated amorphous carbon. Carbon N Y 2016;105:163–75. doi:10.1016/j.carbon.2016.04.021.

[68] Peguiron A, Moras G, Walter M, Uetsuka H, Pastewka L, Moseler M. Activation and mechanochemical breaking of C-C bonds initiate wear of diamond (110) surfaces in contact with silica. Carbon N Y 2016;98:474–83. doi:10.1016/j.carbon.2015.10.098.

[69] Rani R, Panda K, Kumar N, Sankaran KJ, Pandian R, Ficek M, et al. Triboenvironment Dependent Chemical Modification of Sliding Interfaces in Ultrananocrystalline Diamond Nanowall Film: Correlation with Friction and Wear. J Phys Chem C 2018;122:945–56. doi:10.1021/acs.jpcc.7b10992.

[70] Marino MJ, Hsiao E, Chen Y, Eryilmaz OL, Erdemir A, Kim SH. Understanding Run-In Behavior of Diamond-Like Carbon Friction and Preventing Diamond-Like Carbon Wear in Humid Air 2011:12702–8.

[71] Scharf TW, Singer IL. Role of third bodies in friction behaviour of diamond-like nanocomposites coatings studied by In Situ tribometry. Tribol Trans 2002;45:363–71. doi:10.1080/10402000208982561.

[72] Santiago JA, Fernández-Martínez I, Sánchez-López JC, T.C. Rojas, Wennberg A, Bellido-González V, et al. Tribomechanical properties of hard Cr-doped DLC coatings deposited by low-frequency HiPIMS. Surf Coatings Technol 2019:124899.

[73] Jantschner O, Field SK, Music D, Terziyska VL, Schneider JM, Munnik F, et al. Sputtered Si-containing low-friction carbon coatings for elevated temperatures. Tribol Int 2014;77:15–23. doi:10.1016/j.triboint.2014.04.006.

[74] Dai W, Ke P, Wang A. Microstructure and property evolution of Cr-DLC films with different Cr content deposited by a hybrid beam technique. Vacuum 2011;85:792–7. doi:10.1016/j.vacuum.2010.11.013.

[75] Boubiche N, El Hamouchi J, Hulik J, Abdesslam M, Speisser C, Djeffal F, et al. Kinetics of graphitization of thin diamond-like carbon (DLC) films catalyzed by transition metal. Diam Relat Mater 2019;91:190–8. doi:10.1016/j.diamond.2018.10.025.

[76] Jantschner O, Field SK, Holec D, Fian A, Music D, Schneider JM, et al. Origin of temperature-induced low friction of sputtered Si-containing amorphous carbon coatings. Acta Mater 2015;82:437–46. doi:10.1016/j.actamat.2014.09.030.

[77] Liu H, Tanaka A, Umeda K. The tribological characteristics of diamond-like carbon films at elevated temperatures. Thin Solid Films 1999;346:162–8.

Tables

	Si content (at. %)	Cr content (at. %)	G-peak (cm^{-1})	FWHM (cm^{-1})	I_D / I_G	sp^3 C-C content (%)	H (GPa)	E' (GPa)
a-C:Si	1.3 ± 0.1	0	1557 ± 2	169 ± 2	1.23 ± 0.10	22.5 ± 0.8	16.1 ± 1.0	182.7 ± 7.0
a-C:Si,Cr (1)	1.4 ± 0.1	0.3 ± 0.1	1559 ± 1	165 ± 1	1.39 ± 0.01	20.9 ± 0.2	13.5 ± 0.8	160.0 ± 6.3
a-C:Si,Cr (2)	1.5 ± 0.2	2.7 ± 0.3	1565 ± 2	147 ± 1	1.55 ± 0.06	18.0 ± 0.4	10.4 ± 0.8	145.4 ± 6.0

Table 1.

Atomic content of the dopants, Raman parameters extracted from the fitting of the Raman spectra, sp^3 C-C content of the films obtained from XPS, hardness and reduced Young's modulus values for each of the films investigated.

Figure captions

Figure 1.

XPS core-level spectra of the Si 2*p* orbital for all the films: (a) Non Ar^+ sputtered at room temperature, (b) Ar^+ sputtered at room temperature.

Figure 2.

Raman spectra of a-C:Si, a-C:Si,Cr (1) and a-C:Si,Cr (2) at room temperature.

Figure 3.

Analysis of the Raman spectra for each studied film as a result of the annealing temperature. (a) FWHM of the G peak; (b) G peak position; (c) Intensity ratio between D and G peaks. Note: when the error bars are not visible, their size is smaller than the markers.

Figure 4.

XPS core-level spectra of the Si 2*p* orbital for all the films studied in the present work under 250 °C annealing for 15 minutes.

Figure 5.

Bar diagram of the (a) steady state coefficient of friction during the last 1000 strokes; (b) specific wear rate as function of temperature for the ball-on-disk tests carried out on a-C:Si, a-C:Si,Cr (1) and a-C:Si,Cr (2) against Al_2O_3. Note that each bar represents the average value of at least two tests performed at each temperature for the coefficient of friction, while the error bars in the specific wear rate were obtained by four measurements in different areas across each of the studied wear tracks for each temperature. * Failure of coating.

Figure 6.

Variation of the coefficient of friction with the number of strokes using 6.3 mm diameter Al_2O_3 balls as counterpart, 10 N load and 1 cm/s linear speed at (a) 25 °C, (b) 150 °C, (c) 200 °C, (d) 250 °C, (e) 300 °C, (f) 350 °C.

Figure 7.

3D surface profiles of the wear tracks for each of the specimens were included with the scale bar ranging from + 1 µm (orange-red) to -2 µm (purple-wine). At the higher temperature, a star refers to a variation in the scale due to the failures, ranging from +1 µm to -12 µm.

Figure 1.

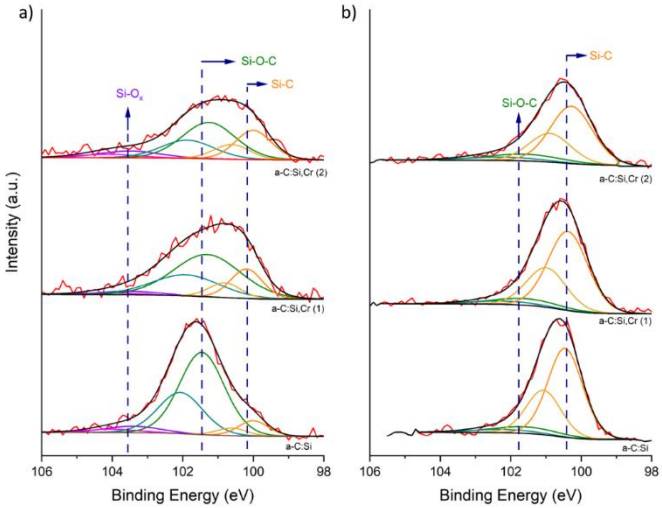
a)
b)
Si-O-C
Si-C
Si-O$_x$
a-C:Si,Cr (2)
a-C:Si,Cr (1)
a-C:Si
Intensity (a.u.)
106
104
102
100
98
Binding Energy (eV)

Figure 2.

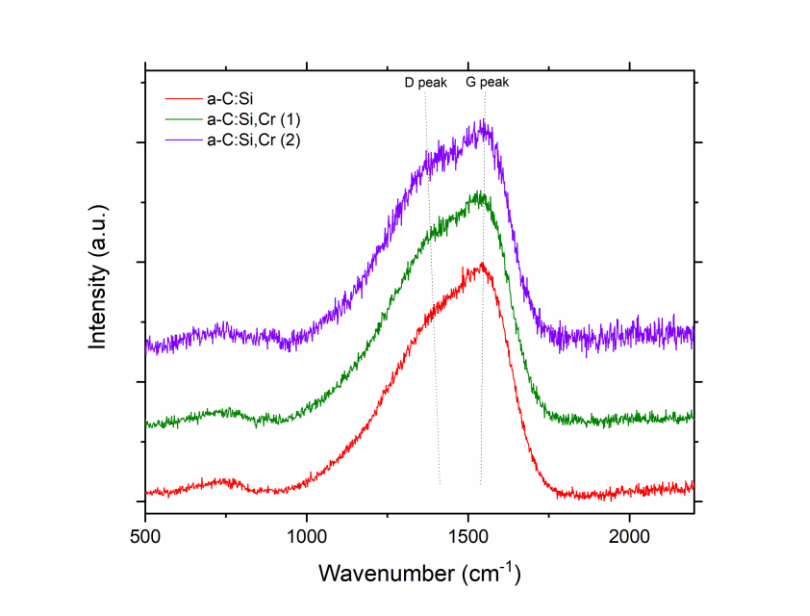
D peak
G peak
a-C:Si
a-C:Si,Cr (1)
a-C:Si,Cr (2)
Intensity (a.u.)
500
1000
1500
2000
Wavenumber (cm-1)

Figure 3.

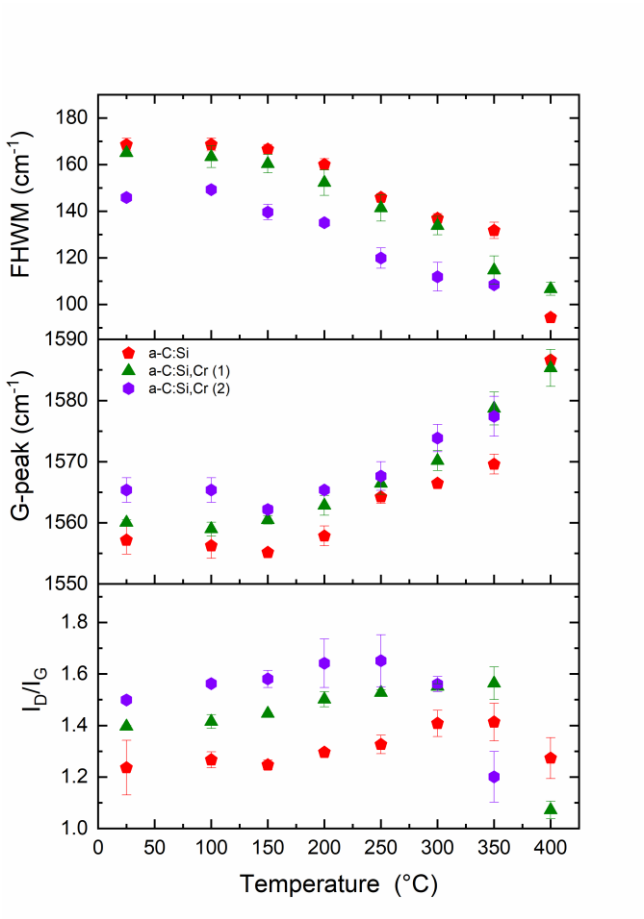

Figure 4.

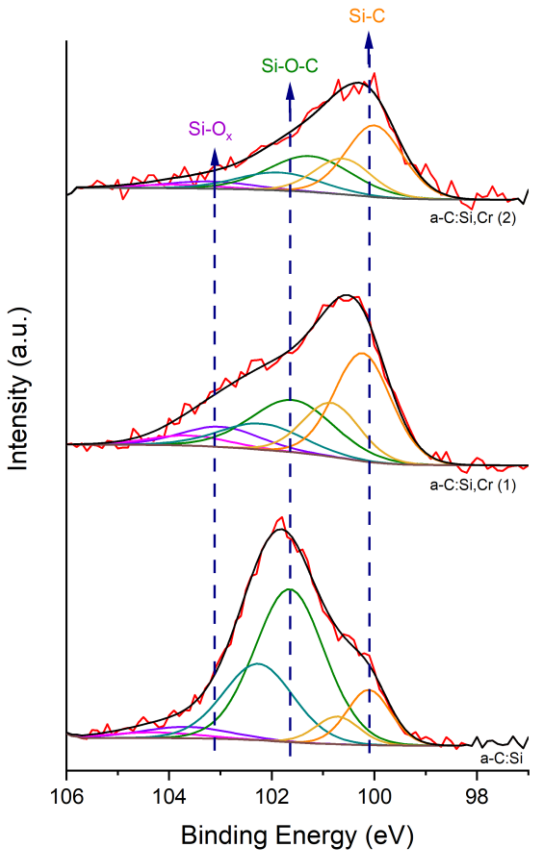
Si-C
Si-O-C
Si-O$_x$
a-C:Si,Cr (2)
a-C:Si,Cr (1)
a-C:Si
Intensity (a.u.)
106
104
102
100
98
Binding Energy (eV)

Figure 5.

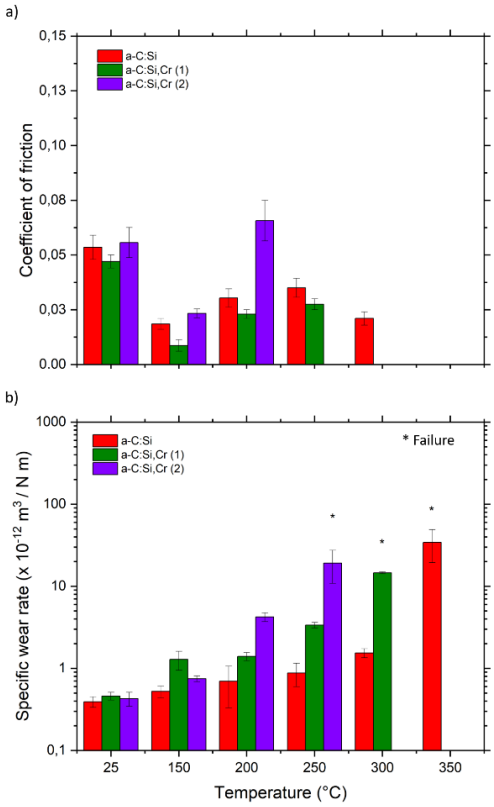
a)
0,15
0,13
0,10
0,08
0,05
0,03
0.00
Coefficient of friction
a-C:Si
a-C:Si,Cr (1)
a-C:Si,Cr (2)
b)
1000
100
10
1
0,1
Specific wear rate (x 10-12 m3 / N m)
a-C:Si
a-C:Si,Cr (1)
a-C:Si,Cr (2)
* Failure
*
*
*
25
150
200
250
300
350
Temperature (°C)

Figure 6.

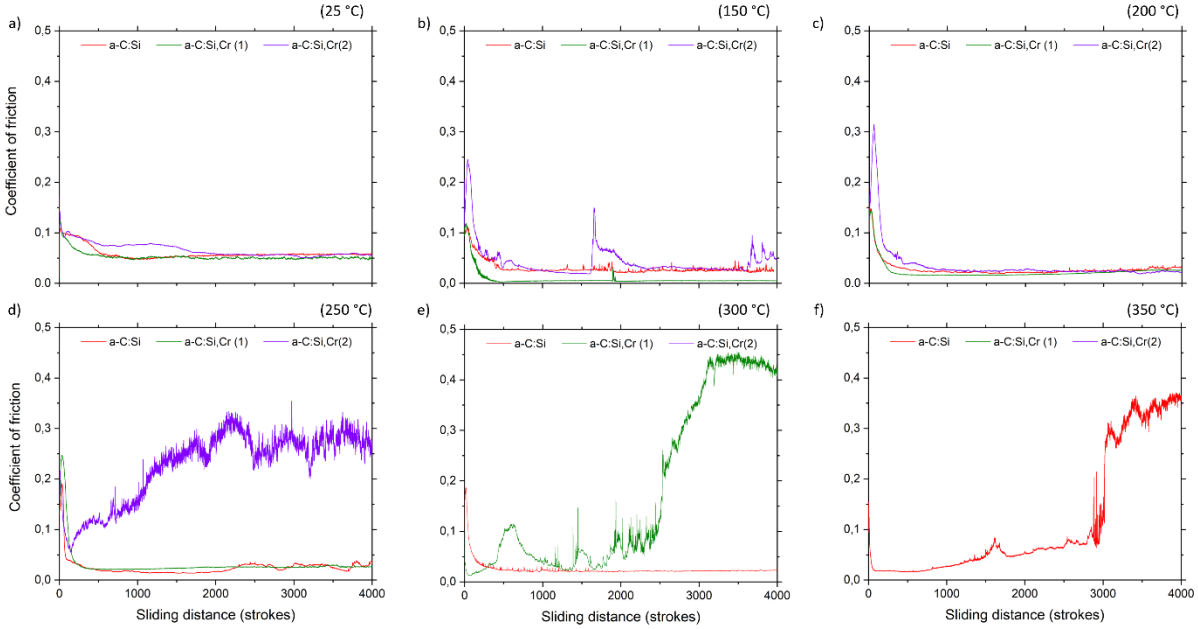
a)
(25 °C)
b)
(150 °C)
c)
(200 °C)
d)
(250 °C)
e)
(300 °C)
f)
(350 °C)
a-C:Si
a-C:Si,Cr (1)
a-C:Si,Cr(2)
Coefficient of friction
Sliding distance (strokes)
0,0
0,1
0,2
0,3
0,4
0,5
0
1000
2000
3000
4000

Figure 7.

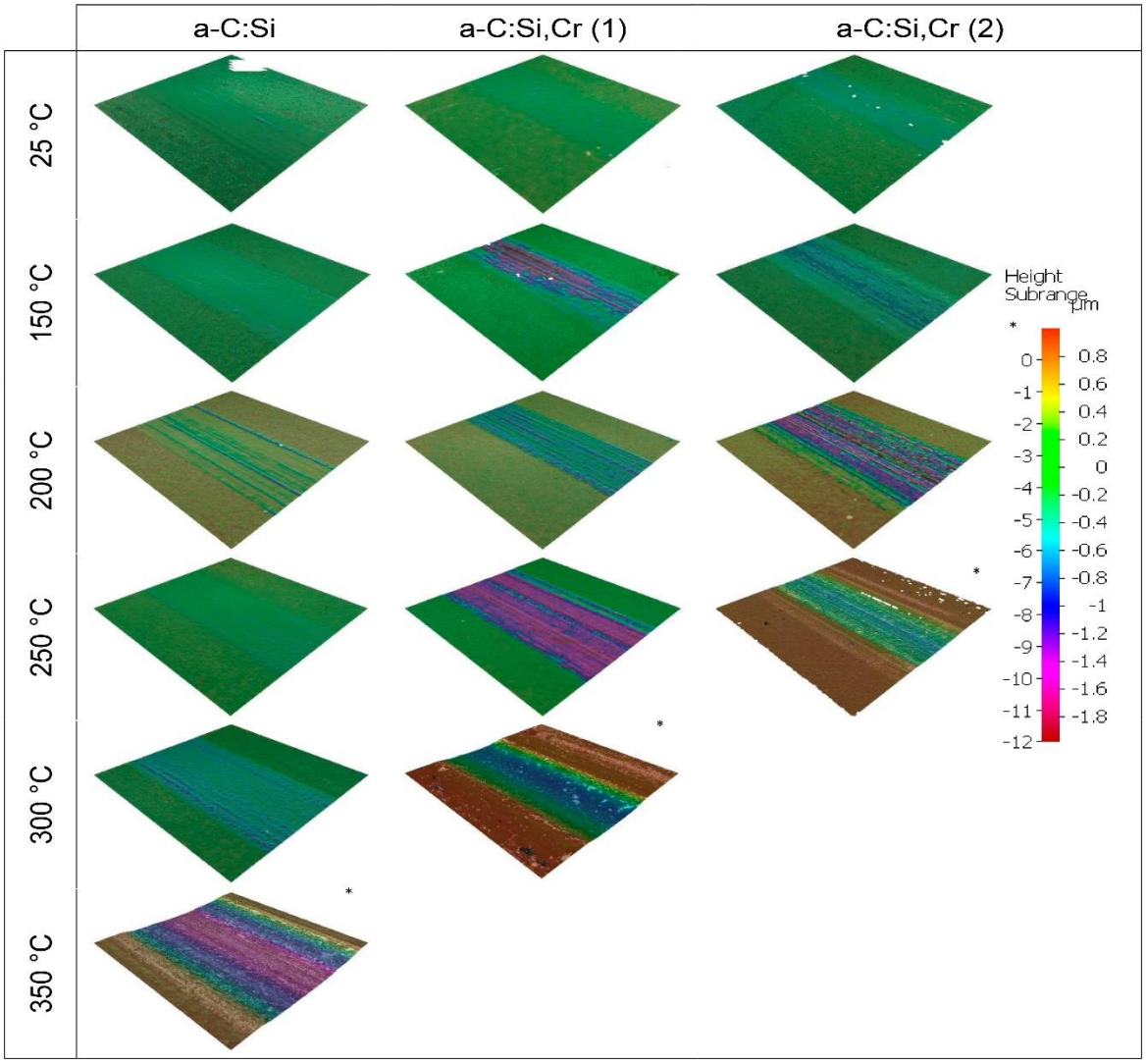
a-C:Si
a-C:Si,Cr (1)
a-C:Si,Cr (2)
25 °C
150 °C
200 °C
250 °C
300 °C
350 °C
Height
Subrange
µm
0
-1
-2
-3
-4
-5
-6
-7
-8
-9
-10
-11
-12
0.8
0.6
0.4
0.2
0
-0.2
-0.4
-0.6
-0.8
-1
-1.2
-1.4
-1.6
-1.8